

# Uncertainty propagation in feed-forward neural network models

Jeremy Diamzon<sup>a</sup>, Daniele Venturi<sup>a,\*</sup>

<sup>a</sup>*Department of Applied Mathematics, UC Santa Cruz, Santa Cruz, CA 95064*

---

## Abstract

We develop new uncertainty propagation methods for feed-forward neural network architectures with leaky ReLU activation functions subject to random perturbations in the input vectors. In particular, we derive analytical expressions for the probability density function (PDF) of the neural network output and its statistical moments as a function of the input uncertainty and the parameters of the network, i.e., weights and biases. A key finding is that an appropriate linearization of the leaky ReLU activation function yields accurate statistical results even for large perturbations in the input vectors. This can be attributed to the way information propagates through the network. We also propose new analytically tractable Gaussian copula surrogate models to approximate the full joint PDF of the neural network output. To validate our theoretical results, we conduct Monte Carlo simulations and a thorough error analysis on a multi-layer neural network representing a nonlinear integro-differential operator between two polynomial function spaces. Our findings demonstrate excellent agreement between the theoretical predictions and Monte Carlo simulations.

---

## 1. Introduction

In the past decade, the field of Scientific Machine Learning (SciML) has made remarkable advancements influencing a wide range of disciplines, including physics, engineering, and medicine [1, 4, 8]. However, despite these advancements, an effective framework to assess the reliability and trustworthiness of solutions generated by neural network models has lagged behind their rapidly evolving capabilities. This gap is particularly pronounced in applications involving partial differential equations (PDEs) [14, 11], and operator mappings between infinite-dimensional function spaces [13, 20, 17, 15, 12], where even small uncertainties in input variables or parameters can be amplified by the neural network, resulting in inaccurate predictions.

In general, uncertainty in neural network models may be categorized into *aleatoric* uncertainty, which arises from inherent variability or noise within the data, and *epistemic* uncertainty, which stems from model limitations or insufficient knowledge [1, 4, 16]. Quantifying the effects of these uncertainties is critical in fields where reliable predictions are essential, and the consequences of inaccurate outcomes can be severe. Nonetheless, despite significant progress in incorporating uncertainty quantification (UQ) methods into data-driven and physics-informed learning frameworks, their effective integration into the broader field of SciML is still in its early stages.

In this paper, we develop new uncertainty propagation methods for feed-forward neural network architectures representing a nonlinear (non-local) operator between two polynomial function spaces [20]. We write such operator as

$$g(y) = \mathcal{N}(f(x)), \quad (1)$$

and assume that  $f(x)$  is a random polynomial with given statistical properties. The goal is to study the statistical properties of the output function  $g(y)$ , such as its mean, covariance, and multi-point probability

---

\*Corresponding author

*Email addresses:* `jdiamzon@ucsc.edu` (Jeremy Diamzon), `venturi@ucsc.edu` (Daniele Venturi)

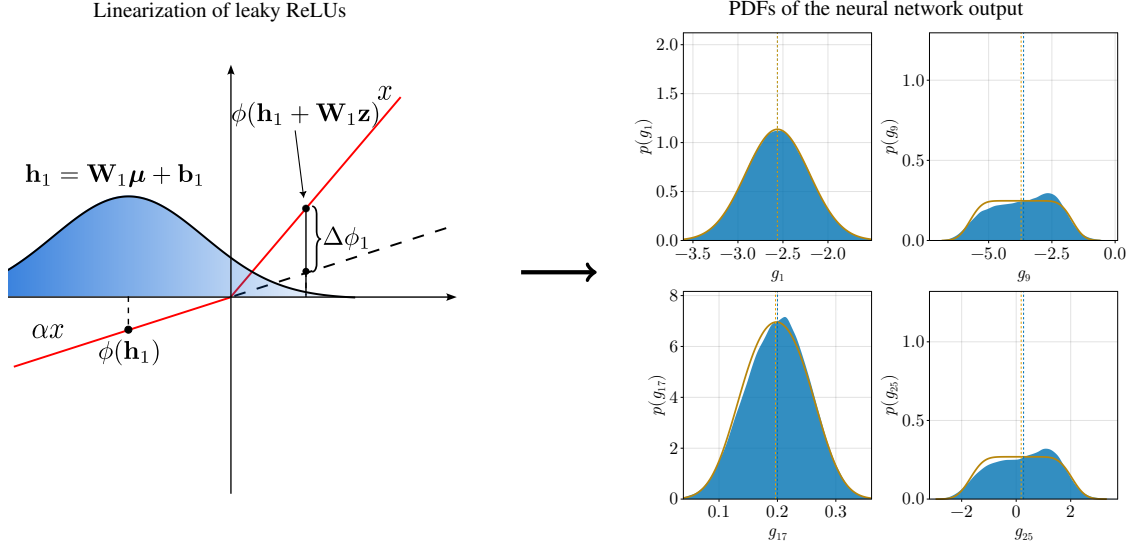


Figure 1: Illustration of the linearization of the leaky ReLU activation function  $\phi(\cdot)$  for a one-layer neural network. The neuron input  $\mathbf{h}_1 = \mathbf{W}_1\boldsymbol{\mu} + \mathbf{b}_1$  is perturbed to  $\mathbf{h}_1 + \mathbf{W}_1\mathbf{z}$ , where  $\{\mathbf{W}_1, \mathbf{b}_1\}$  are weights and biases of the first layer, and  $\mathbf{z}$  is vector representing the random perturbation of the input function  $f(x)$  (see Eq. 4). The PDF of  $\mathbf{h}_1 + \mathbf{W}_1\mathbf{z}$  is sketched as a Gaussian in Figure. The leaky ReLU function is linearized at  $\mathbf{h}_1$ . Its extension to the positive real axis is represented by the black dashed line. If the samples of  $\mathbf{h}_1 + \mathbf{W}_1\mathbf{z}$  are negative, there is no difference between the output of the linearized leaky ReLU and the ReLU function. However, if the samples of  $\mathbf{h}_1 + \mathbf{W}_1\mathbf{z}$  are positive then the linearized leaky ReLU approximation introduces an error  $\Delta_1\phi(\mathbf{h}_1)$ . The cumulative effect of these errors tends to cancel out for deep nets as they propagate through the network, preserving accuracy in the one-point PDFs of the neural network output function  $g(y)$ .

density functions (PDFs), when the operator  $\mathcal{N}$  is approximated using a deep neural network with leaky ReLU activation functions. A key finding of our study is that a linearization of the leaky ReLU activation function in the deep net representing (1) allows us to obtain *computable analytical expressions* for the PDF of the output function  $g(y)$  and its statistical moments (see Figure 1). Such analytical expressions turn out to be accurate for *large perturbations* in the input function  $f(x)$ . Furthermore, we show that multi-point PDFs of the output function  $g(y)$  can be accurately approximated by a *Gaussian copula* [3], which can be constructed based on the analytical formulas we obtain for the marginal distribution of  $g(y_i)$  (one-point PDFs), and the correlation function  $\mathbb{E}\{g(y_i)g(y_j)\}$ . In other words, the uncertainty in the output function  $g(y)$  can be rigorously quantified using analytical expressions for its PDFs and statistical moments, for any given fully connected feed-forward neural network, and a statistical characterization of the random input function  $f(x)$ .

This paper is organized as follows. In Section 2 we formulate the operator approximation problem, including the discretization of the input-output functions and the mapping between the input and the output. In Section 3, we model fully connected feed-forward neural networks as discrete dynamical systems and set the mathematical foundations for our approximation methods. In Section 4 we derive analytical expressions for the PDF of the neural network output. In Section 5, we extend the analysis to compute statistical moments such as the mean, variance, and covariance of the network output. To obtain these expressions, we introduce a suitable linearization of the leaky ReLU activation function, which makes the analytical formulas for both the PDF and the moments tractable and computable. In Section 6 we introduce a new Gaussian copula model to approximate the full joint distribution of the network output based on the derived analytical expressions for the marginal PDFs and the correlation function. In Section 7 we present numerical results that validate our theoretical predictions across a range of scenarios, including both linear and nonlinear operators. The main findings of this study are summarized in Section 8. Additional technical details, including the derivation of

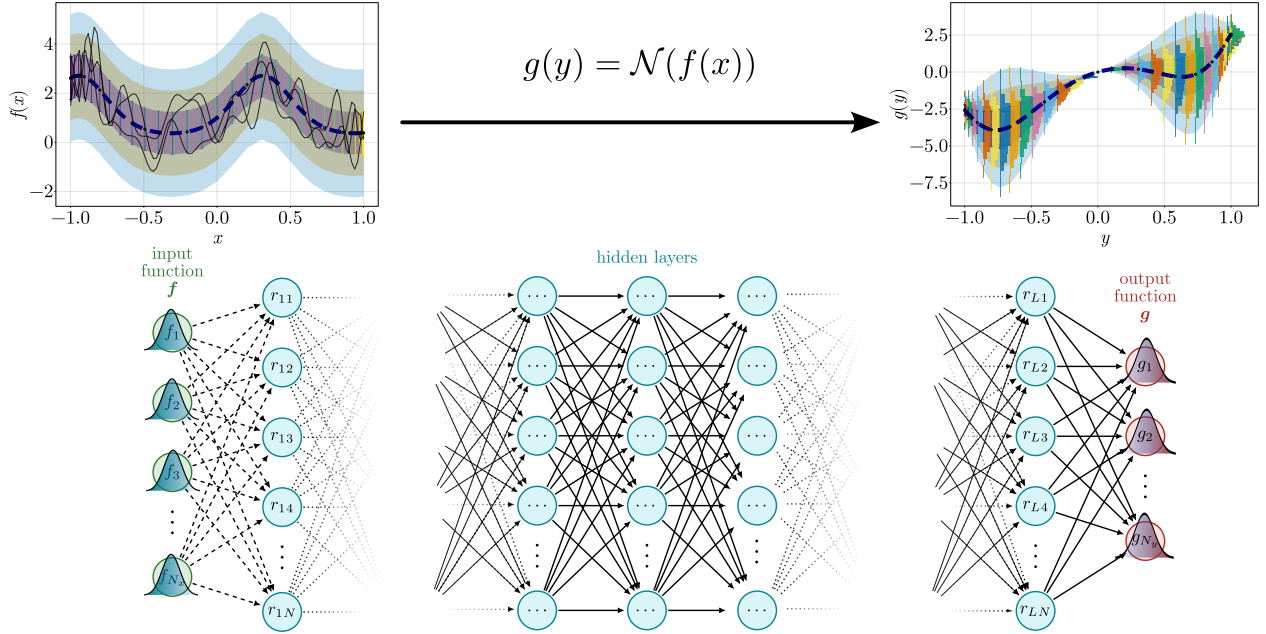


Figure 2: Schematic of the feed-forward neural network approximating the non-linear (non-local) operator  $g(y) = \mathcal{N}(f(x))$ . The input function is assumed to be random, with known probability distribution. This makes the output function  $g(y)$  random. The goal is to study the statistical properties of  $g(y)$  given statistical information on  $f(x)$  and the parameters defining the neural net.

the PDF of the neural network output for linearized leaky ReLU activations functions and an error analysis for linearized leaky ReLU networks are presented in Appendix A and Appendix B, respectively.

## 2. Problem Formulation

We are interested in computing the statistical properties, e.g. statistical moments and PDF of the output, of a neural network approximating the nonlinear operator (1), given statistical information on the input. To this end, we first select two appropriate polynomial function spaces defined on two intervals that are large enough to accommodate all input-output function pairs  $\{f(x), g(y)\}$  of interest. Such input/output functions are then represented as Lagrangian interpolants at shifted Gauss-Legendre-Lobatto [5] grid points  $\{x_1, \dots, x_{N_x}\}$  and  $\{y_1, \dots, y_{N_y}\}$ . This reduces the input-output function pairs  $\{f(x), g(y)\}$  to a set of input-output vectors

$$\mathbf{f} = [f_1 \ \cdots \ f_{N_x}], \quad \mathbf{g} = [g_1 \ \cdots \ g_{N_y}], \quad (2)$$

with components

$$f_i = f(x_i) \quad (i = 1, \dots, N_x) \quad \text{and} \quad g_j = g(y_j) \quad (j = 1, \dots, N_y). \quad (3)$$

This reduces the problem of learning a nonlinear operator between two Banach spaces to the problem of learning a nonlinear map between two finite-dimensional vector spaces, i.e., a map from  $\mathbb{R}^{N_x}$  to  $\mathbb{R}^{N_y}$ . In what follows, it is convenient to model the random input vector  $\mathbf{f}$  as the sum of a mean vector  $\boldsymbol{\mu}$  and a superimposed zero-mean random perturbation  $\mathbf{z}$ , i.e.,

$$\mathbf{f} = \boldsymbol{\mu} + \mathbf{z}. \quad (4)$$

The perturbation  $\mathbf{z}$  may or may not be small and requires a probabilistic description. For instance,  $\mathbf{z}$  may be modeled as a zero-mean jointly Gaussian vector with a specified covariance matrix, or as a vector with

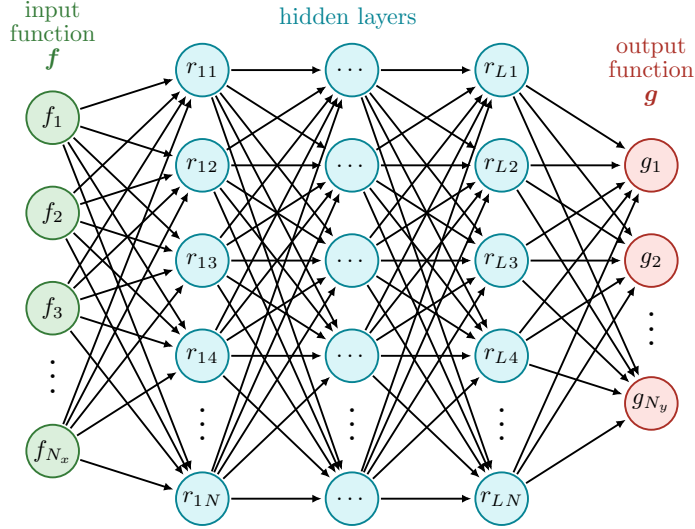


Figure 3: Schematic of the fully connected feed-forward (MLP) neural network used in this study.

independent and identically distributed (i.i.d.) components following a uniform distribution on the interval  $[-\beta, \beta]$ . In the latter case, the joint PDF of  $\mathbf{z}$  is given by

$$p(\mathbf{z}) = \begin{cases} \frac{1}{(2\beta)^{N_x}} & \text{if } \mathbf{z} \in [-\beta, \beta]^{N_x} \\ 0 & \text{otherwise} \end{cases} \quad (5)$$

where  $\beta$  controls the amplitude of the perturbation in the input vector, which may be large (see Figure 4).

### 3. Modeling feed-forward neural networks as discrete dynamical systems

The input-output map representing the nonlinear operator (1) is chosen as a fully connected feed-forward neural network with  $L$  hidden layers. As is well known [18, 9], such neural network can be modeled as a discrete dynamical system via the following recurrence relation (see Figure 3)

$$\mathbf{r}_1 = \mathcal{F}_1(\mathbf{f}; \Theta_1), \quad \dots \quad \mathbf{r}_{n+1} = \mathcal{F}_{n+1}(\mathbf{r}_n; \Theta_n), \quad n = 1, \dots, L. \quad (6)$$

Here,  $\mathbf{f} \in \mathbb{R}^{N_x}$  is the vector representing the random input function  $f(x)$ ,  $\Theta_n$  are the set of neural network parameters for the  $n$ -th layer, usually consisting of weight and bias parameters  $\{\mathbf{W}_n, \mathbf{b}_n\}$ , where  $\mathbf{W}_n \in \mathbb{R}^{N \times N}$ ,  $\mathbf{W}_1 \in \mathbb{R}^{N \times N_x}$ ,  $\mathbf{b}_n \in \mathbb{R}^N$ , and  $\mathbf{r}_n \in \mathbb{R}^N$  ( $n = 1, \dots, L$ ).

The operator  $\mathcal{F}_n$  represents the mapping from the  $n$ -th hidden layer to the subsequent layer. Its form varies depending on the type of neural network being considered, e.g., fully connected networks (MLPs), convolutional neural networks (CNNs), and residual networks (ResNets), among others. In the simple fully-connected feed-forward net setting we consider here,  $\mathcal{F}_n$  takes the following recurrent form across all  $L$  layers

$$\mathcal{F}_n(\mathbf{r}_{n-1}; \Theta_n) := \phi_n(\mathbf{W}_n \mathbf{r}_{n-1} + \mathbf{b}_n) \quad n = 1, \dots, L, \quad (7)$$

where  $\phi_n : \mathbb{R} \rightarrow \mathbb{R}$  is the activation function at the  $n$ -th layer. In this paper, we assume that the activation function is the same across all layers, i.e. we set  $\phi_n = \phi$  for all  $n = 1, \dots, L$ , and select a leaky rectified

linear unit (ReLU), a piecewise-linear variant of the standard ReLU function, defined as<sup>1</sup>

$$\phi(x) = \begin{cases} x & x \geq 0 \\ \alpha x & \text{otherwise} \end{cases}. \quad (8)$$

Note that  $\phi(x)$  can be expressed in terms of the Heaviside step function  $H(x)$  as

$$\phi(x) = H(x)x + \alpha(1 - H(x))x. \quad (9)$$

The network output is represented by a linear layer represented by a matrix  $\mathbf{A} \in \mathbb{R}^{N_y \times N}$ , with trainable entries, where  $N_y$  is the the number of grid points we use to represent the output function  $g(y)$ . This allows us to write the fully discrete input-output map as

$$\begin{aligned} \mathbf{g} &= \mathbf{A}\mathcal{F}_L(\mathbf{r}_{L-1}; \Theta_L) \\ &= \mathbf{A}\mathcal{F}_L \circ \mathcal{F}_{L-1} \circ \cdots \circ \mathcal{F}_2 \circ \mathcal{F}_1(\mathbf{f}; \Theta_1). \end{aligned} \quad (10)$$

Equation (10) can be written explicitly for one-, two-, and  $L$ -layers as follows

$$\mathbf{g} = \mathbf{A}\phi(\mathbf{W}_1\mathbf{f} + \mathbf{b}_1), \quad (11)$$

$$\mathbf{g} = \mathbf{A}\phi(\mathbf{W}_2\phi(\mathbf{W}_1\mathbf{f} + \mathbf{b}_1) + \mathbf{b}_2), \quad (12)$$

$\vdots$

$$\mathbf{g} = \mathbf{A}\phi(\mathbf{W}_L\phi(\mathbf{W}_{L-1}\phi(\cdots\phi(\mathbf{W}_1\mathbf{f} + \mathbf{b}_1)\cdots) + \mathbf{b}_{L-1}) + \mathbf{b}_L). \quad (13)$$

#### 4. PDF of the neural network output

The sequence of vectors  $\{\mathbf{f}, \mathbf{r}_1, \mathbf{r}_2, \dots, \mathbf{r}_L, \mathbf{g}\}$  forms a discrete Markov process. Hence, the joint probability density function (PDF) of the random vectors  $(\mathbf{g}, \mathbf{r}_L, \dots, \mathbf{r}_1, \mathbf{f})$ , i.e., joint PDF of the state of the entire neural network (including input, output, and hidden states), can be factored out as

$$p(\mathbf{g}, \mathbf{r}_L, \dots, \mathbf{r}_1, \mathbf{f}) = p(\mathbf{g}|\mathbf{r}_L)p(\mathbf{r}_L|\mathbf{r}_{L-1})p(\mathbf{r}_{L-1}|\mathbf{r}_{L-2})\cdots p(\mathbf{r}_1|\mathbf{f})p(\mathbf{f}) \quad (14)$$

where  $p(\mathbf{f})$  is the joint probability density function of the random input vector  $\mathbf{f}$ . The transition densities  $p(\mathbf{g}|\mathbf{r}_L)$ ,  $p(\mathbf{r}_n|\mathbf{r}_{n-1})$  and  $p(\mathbf{r}_1|\mathbf{f})$  can be easily expressed as in terms of multivariate Dirac delta functions as

$$p(\mathbf{g}|\mathbf{r}_L) = \delta(\mathbf{g} - \mathbf{A}\mathbf{r}_L), \quad (15)$$

$$p(\mathbf{r}_n|\mathbf{r}_{n-1}) = \delta(\mathbf{r}_n - \phi(\mathbf{W}_n\mathbf{r}_{n-1} + \mathbf{b}_n)), \quad (16)$$

$$p(\mathbf{r}_1|\mathbf{f}) = \delta(\mathbf{r}_1 - \phi(\mathbf{W}_1\mathbf{f} + \mathbf{b}_1)). \quad (17)$$

By integrating (14) relative to the phase variables  $\{\mathbf{f}, \mathbf{r}_1, \dots, \mathbf{r}_L\}$  we can easily express the PDF of the output  $\mathbf{g}$  in terms for the PDF of the input  $\mathbf{f}$ . For instance, for a one-layer network we have

$$p(\mathbf{g}) = \int_{\mathbb{R}^{N_x}} \delta(\mathbf{g} - \mathbf{A}\phi(\mathbf{W}_1\mathbf{f} + \mathbf{b}_1))p(\mathbf{f})d\mathbf{f}. \quad (18)$$

We can write the multivariate Dirac delta at the right hand side of (18) in a Fourier form as

$$\delta(\mathbf{g} - \mathbf{A}\phi(\mathbf{W}_1\mathbf{f} + \mathbf{b}_1)) = \frac{1}{(2\pi)^{N_y}} \int_{\mathbb{R}^{N_y}} e^{i\mathbf{a}\cdot[\mathbf{g} - \mathbf{A}\phi(\mathbf{W}_1\mathbf{f} + \mathbf{b}_1)]}d\mathbf{a}. \quad (19)$$

---

<sup>1</sup>We set  $\alpha = 0.01$  in (8).

Substituting this expression into (18) yields the following input-output PDF map

$$p(\mathbf{g}) = \frac{1}{(2\pi)^{N_y}} \int_{\mathbb{R}^{N_y}} \int_{\mathbb{R}^{N_x}} e^{i\mathbf{a} \cdot [\mathbf{g} - \mathbf{A}\phi(\mathbf{W}_1\mathbf{f} + \mathbf{b}_1)]} p(\mathbf{f}) d\mathbf{f} d\mathbf{a}. \quad (20)$$

Note that the PDF of  $\mathbf{g}$  depends on the weights and biases of the first layer, the leaky ReLU activation function  $\phi(\cdot)$ , and the PDF of the input  $p(\mathbf{f})$ . Similarly, the input-output PDF map for a network with two layers can be written as

$$p(\mathbf{g}) = \frac{1}{(2\pi)^{N_y}} \int_{\mathbb{R}^{N_y}} \int_{\mathbb{R}^{N_x}} e^{i\mathbf{a} \cdot [\mathbf{g} - \mathbf{A}\phi(\mathbf{W}_2\phi(\mathbf{W}_1\mathbf{f} + \mathbf{b}_1) + \mathbf{b}_2)]} p(\mathbf{f}) d\mathbf{f} d\mathbf{a}. \quad (21)$$

This can be easily generalized to networks with  $L$  layers as

$$p(\mathbf{g}) = \frac{1}{(2\pi)^{N_y}} \int_{\mathbb{R}^{N_y}} \int_{\mathbb{R}^{N_x}} e^{i\mathbf{a} \cdot [\mathbf{g} - \mathbf{A}\phi(\mathbf{W}_L\phi(\mathbf{W}_{L-1}\phi(\dots\phi(\mathbf{W}_1\mathbf{f} + \mathbf{b}_1)\dots) + \mathbf{b}_{L-1}) + \mathbf{b}_L)]} p(\mathbf{f}) d\mathbf{f} d\mathbf{a}. \quad (22)$$

#### 4.1. Linearization of leaky ReLUs

While equations (20)-(22) are *exact*, their analytical computation, i.e., the computation of the integrals, may be intractable. Hence, we introduce an approximation that significantly simplifies the analysis, i.e., we linearize the leaky ReLU activation functions at the mean  $\boldsymbol{\mu}$  of the random input vector  $\mathbf{f} = \boldsymbol{\mu} + \mathbf{z}$  (see Eq. (4)). For a network with one layer we obtain

$$\phi(\mathbf{W}_1(\boldsymbol{\mu} + \mathbf{z}) + \mathbf{b}_1) \simeq \phi(\mathbf{W}_1\boldsymbol{\mu} + \mathbf{b}_1) + \phi'(\mathbf{W}_1\boldsymbol{\mu} + \mathbf{b}_1) \boxtimes \mathbf{W}_1\mathbf{z}, \quad (23)$$

where  $\boxtimes$  is a variant of the Khatri-Rao product known as the *face-splitting product*<sup>2</sup>,  $\phi'(\cdot)$  is the first derivative of the leaky ReLU activation function (8)

$$\phi'(x) = \begin{cases} 1 & x > 0 \\ \alpha & x < 0 \end{cases}, \quad (26)$$

and  $\mathbf{z}$  is the random component in the input vector  $\mathbf{f}$  (see Eq. (4)). Equation (23) can be written in compact form as

$$\phi(\mathbf{W}_1(\boldsymbol{\mu} + \mathbf{z}) + \mathbf{b}_1) \simeq \phi(\mathbf{W}_1\boldsymbol{\mu} + \mathbf{b}_1) + \mathbf{J}_1\mathbf{z}, \quad (27)$$

where

$$\mathbf{J}_1 = \phi'(\mathbf{W}_1\boldsymbol{\mu} + \mathbf{b}_1) \boxtimes \mathbf{W}_1. \quad (28)$$

The advantage of using this notation is that it holds for multiple layers as well. For instance, it can be shown that for a network with two layers we have

$$\phi(\mathbf{W}_2\phi(\mathbf{W}_1(\boldsymbol{\mu} + \mathbf{z}) + \mathbf{b}_1) + \mathbf{b}_2) \simeq \phi(\mathbf{W}_2\phi(\mathbf{W}_1\boldsymbol{\mu} + \mathbf{b}_1) + \mathbf{b}_2) + \mathbf{J}_2\mathbf{z}, \quad (29)$$

<sup>2</sup>Given an  $m \times n$  matrix  $\mathbf{X}$  (with rows  $\mathbf{X}_i$ ) and an  $m \times p$  matrix  $\mathbf{Y}$  (with rows  $\mathbf{Y}_i$ )

$$\mathbf{X} = \begin{bmatrix} \mathbf{X}_1 \\ \vdots \\ \mathbf{X}_m \end{bmatrix}, \quad \mathbf{Y} = \begin{bmatrix} \mathbf{Y}_1 \\ \vdots \\ \mathbf{Y}_m \end{bmatrix}, \quad (24)$$

the face-splitting product between  $\mathbf{X}$  and  $\mathbf{Y}$  is defined as their corresponding row-wise Kronecker product. This results in the following  $m \times np$  matrix

$$\mathbf{X} \boxtimes \mathbf{Y} = \begin{bmatrix} \mathbf{X}_1 \otimes \mathbf{Y}_1 \\ \vdots \\ \mathbf{X}_m \otimes \mathbf{Y}_m \end{bmatrix} \quad (25)$$

where

$$\mathbf{J}_2 = [\phi'(\mathbf{W}_2\phi(\mathbf{W}_1\boldsymbol{\mu} + \mathbf{b}_1) + \mathbf{b}_2) \square \mathbf{W}_2] \phi'(\mathbf{W}_1\boldsymbol{\mu} + \mathbf{b}_1) \square \mathbf{W}_1. \quad (30)$$

These expressions can be readily extended to networks with  $L$  layers by induction. In essence,  $\mathbf{J}_L$  is a product of neural network Jacobians (readily computed via backpropagation) multiplied by  $\mathbf{W}_j$  through the face-splitting product, i.e.,

$$\begin{aligned} \mathbf{J}_L &= [\phi'(\mathbf{W}_L\phi(\mathbf{W}_{L-1}\phi(\cdots\phi(\mathbf{W}_1\boldsymbol{\mu} + \mathbf{b}_1)\cdots) + \mathbf{b}_{L-1}) + \mathbf{b}_L) \square \mathbf{W}_L] \cdots \\ &[\phi'(\mathbf{W}_2\phi(\mathbf{W}_1\boldsymbol{\mu} + \mathbf{b}_1) + \mathbf{b}_2) \square \mathbf{W}_2] \phi'(\mathbf{W}_1\boldsymbol{\mu} + \mathbf{b}_1) \square \mathbf{W}_1. \end{aligned} \quad (31)$$

#### 4.2. Approximation of the PDF of the neural network output

With the the linearized composition of leaky ReLU available, we can now compute analytically the approximated PDF of the  $j$ -th component of the output  $g_j$ . In Appendix A we show that for uniformly distributed inputs vectors  $\mathbf{f} = \boldsymbol{\mu} + \mathbf{z}$  with  $p(\mathbf{z})$  given in (5), the PDF  $p(g_j)$  can be expressed as a *convolution of rectangular functions*. Specifically,

$$p(g_j) = \frac{1}{2\pi} \left( \prod_{n=1}^{N_x} \frac{2\pi}{q_{jn}} \right) \Pi_{\beta q_{j1}}[\eta(g_j)] * \cdots * \Pi_{\beta q_{jN_x}}[\eta(g_j)] \quad (32)$$

where

$$\mathbf{q}_j = \mathbf{A}_j \mathbf{J}_L, \quad (33)$$

is a row vector with  $N_x$  components,  $\mathbf{A}_j$  is the  $j$ -th row of the output matrix  $\mathbf{A}$ ,  $\mathbf{J}_L$  is the matrix (31),

$$\eta(g_j) = g_j - \mathbf{A}_j \cdot \phi(\mathbf{W}_L\phi(\mathbf{W}_{L-1}\phi(\cdots\phi(\mathbf{W}_1\boldsymbol{\mu} + \mathbf{b}_1)\cdots) + \mathbf{b}_{L-1}) + \mathbf{b}_L), \quad (34)$$

$\beta$  is the ‘‘perturbation amplitude’’ (see Eq. (5)),  $*$  is standard convolution operation, and  $\Pi_{\beta q_{j1}}(\cdot)$  is the rectangular function (see Eq. (A.7)). In practice, one may compute  $p(g_j)$  using its inverse Fourier transform representation, which involves a product of  $\text{sinc}(\cdot)$  functions as in (A.4), rather than through the iterated convolution of rectangular functions in (32), which can be more computationally expensive.

In Appendix B we develop a thorough error analysis to quantify the effects of linearizing leaky ReLU activation functions on the neural network output. This analysis provides insight into why the approximate analytical formula (32) and the formulas for the statistical moments derived hereafter in Section 5, remain remarkably accurate even in the presence of large perturbations in the input vector.

## 5. Statistical moments

The linearized leaky ReLU approximation discussed in Section 4.1 allows us to derive simple expressions for the mean and the covariance matrix of the neural network output  $\mathbf{g}$ . To this end, consider the ‘‘unperturbed’’ network output

$$m_j = \mathbf{A}_j \cdot \phi(\mathbf{W}_L\phi(\mathbf{W}_{L-1}\phi(\cdots\phi(\mathbf{W}_1\boldsymbol{\mu} + \mathbf{b}_1)\cdots) + \mathbf{b}_{L-1}) + \mathbf{b}_L). \quad (35)$$

Recalling the linearized leaky ReLU approximation (e.g., Eq. (27)) we can write the neural network output linearized around the input vector  $\boldsymbol{\mu}$  as

$$g_j = m_j + \mathbf{q}_j \cdot \mathbf{z}, \quad (36)$$

where the vector  $\mathbf{q}_j$  is defined in (33). Recalling that  $\mathbf{z}$  is a zero-mean vector, from this expression it follows that

$$\begin{aligned} \mathbb{E}\{g_j\} &= m_j + \mathbf{q}_j \cdot \mathbb{E}\{\mathbf{z}\} \\ &= m_j. \end{aligned} \quad (37)$$

Similarly,

$$\mathbb{E}\{g_i g_j\} = m_i m_j + \mathbf{q}_i \mathbf{Q} \mathbf{q}_j', \quad (38)$$

where the matrix  $\mathbf{Q}$  has entries

$$Q_{ln} = \mathbb{E}\{z_l z_n\} \quad (\text{covariance of the perturbation vector } \mathbf{z}). \quad (39)$$

If we assume that  $\mathbf{z}$  has i.i.d uniform components in  $[-\beta, \beta]^{N_x}$  (see Eq. (5)) then

$$\mathbb{E}\{g_i g_j\} = m_i m_j + \frac{\beta^2}{3} \mathbf{q}_i \cdot \mathbf{q}_j. \quad (40)$$

In this case, the variance of  $g_j$  and the covariance of  $g_i$  and  $g_j$  can be written as

$$\text{Var}(g_j) = \frac{\beta^2}{3} \|\mathbf{q}_j\|_2^2, \quad (41)$$

$$\text{Cov}(g_i, g_j) = \frac{\beta^2}{3} \mathbf{q}_i \cdot \mathbf{q}_j. \quad (42)$$

## 6. Gaussian copula approximation of the PDF of the neural network output

Let us transform each component  $g_i$  of the random vector  $\mathbf{g}$  representing the output of the neural network to a uniform random variable  $u_i$  via the probability mapping

$$u_i = F_i(g_i) \quad i = 1, \dots, N_y, \quad (43)$$

where  $F_i$  is the cumulative distribution function (CDF) of  $g_i$ . A *copula* is defined as the joint cumulative distribution function of  $\mathbf{u} = [u_1, \dots, u_{N_y}]$ , i.e.,  $F_{\mathbf{u}}(u_1, \dots, u_{N_y})$ . Note that such copula is a multivariate CDF defined on the unit cube  $[0, 1]^n$ , which encodes all information about the dependence structure among the components of the random vector  $\mathbf{g}$ . By using the definition (43) it can be shown that

$$F_{\mathbf{u}}(u_1, \dots, u_{N_y}) = F_{\mathbf{g}}\left(F_1^{-1}(u_1), \dots, F_{N_y}^{-1}(u_{N_y})\right), \quad (44)$$

Where  $F_{\mathbf{g}}$  is the joint CDF of the random vector  $\mathbf{g}$ . This equation can be reversed to obtain

$$F_{\mathbf{g}}(g_1, \dots, g_{N_y}) = F_{\mathbf{u}}\left(F_1(g_1), \dots, F_{N_y}(g_{N_y})\right). \quad (45)$$

Indeed, it is always possible write  $F_{\mathbf{g}}(g_1, \dots, g_{N_y})$  in terms of a copula  $F_{\mathbf{u}}(u_1, \dots, u_{N_y})$  and the individual CDFs  $F_i$  of each component  $g_i$ . This result is known as *Sklar's theorem* [3, Theorem 1.9]. By differentiating (45) with respect to  $(z_1, \dots, z_n)$  yields the copula representation of the PDF of  $\mathbf{g}$ , i.e.,

$$p_{\mathbf{g}}(g_1, \dots, g_{N_y}) = p_{\mathbf{u}}(F_1(g_1), \dots, F_{N_y}(g_{N_y})) p_1(g_1) \cdots p_{N_y}(g_{N_y}), \quad (46)$$

where  $p_{\mathbf{u}}(u_1, \dots, u_{N_y})$  is the PDF of the copula, and  $p_j(g_j)$  is the PDF of  $g_j$ .

### 6.1. Gaussian copulas

Gaussian copulas are constructed from a multivariate normal distribution by using simple one-dimensional probability mappings. For a given correlation matrix  $\mathbf{R}$  the Gaussian copula is defined as

$$F_{\mathbf{u}}(u_1, \dots, u_{N_y}) = F_{\mathbf{R}}^{\text{Gauss}}\left(G^{-1}(u_1), \dots, G^{-1}(u_{N_y})\right), \quad (47)$$

where  $F_{\mathbf{R}}^{\text{Gauss}}$  is the CDF of a zero-mean Gaussian with correlation matrix  $\mathbf{R}$ , and  $G$  are one-dimensional CDFs of standard Gaussian variables with zero mean and variance one, i.e.,

$$G(u) = \frac{1}{2} \left[ 1 + \operatorname{erf} \left( \frac{u}{\sqrt{2}} \right) \right]. \quad (48)$$

By differentiating (47) with respect to  $\{u_1, \dots, u_n\}$  we obtain<sup>3</sup>

$$p_{\mathbf{u}}(u_1, \dots, u_{N_y}) = \frac{1}{\sqrt{\det(\mathbf{R})}} \exp \left[ \frac{1}{2} \mathbf{z}_{\mathbf{u}} (\mathbf{I} - \mathbf{R}^{-1}) \mathbf{z}_{\mathbf{u}}^T \right], \quad (50)$$

where

$$\mathbf{z}_{\mathbf{u}} = [G^{-1}(u_1), \dots, G^{-1}(u_{N_y})]. \quad (51)$$

Substituting (50) into (46) yields the Gaussian copula approximation of the PDF of the neural network output  $\mathbf{g}$ . Note that this approximation depends only on the marginal PDFs of the individual components  $g_j$  (see (32)) and the copula correlation matrix  $\mathbf{R}$  is which can be computed, e.g., from (40). To this end, let

$$C_{ij} = \mathbb{E}\{g_i g_j\}. \quad (52)$$

By using the the copula PDF representation we have

$$C_{ij} = \int_{[0,1]^2} F_i^{-1}(u_i) F_j^{-1}(u_j) p_{\mathbf{u}}(u_i, u_j; \rho_{ij}) du_i du_j \quad i, j = 1, \dots, N_y \quad (53)$$

where

$$p_{\mathbf{u}}(u_i, u_j; \rho_{ij}) = \frac{1}{\sqrt{1 - \rho_{ij}^2}} \exp \left[ \frac{1}{2(1 - \rho_{ij}^2)} \left[ 2\rho_{ij} G^{-1}(u_i) G^{-1}(u_j) - \rho_{ij}^2 (G^{-1}(u_j)^2 + G^{-1}(u_i)^2) \right] \right] \quad (54)$$

are 2D marginals<sup>4</sup> of (50), and  $\rho_{ij}$  is the correlation coefficient. Given a target correlation matrix  $C_{ij}$ , e.g., the analytical correlation (40), we can compute the copula correlation coefficients  $\rho_{ij}$  by solving the following sequence of 1D optimization problem

$$\min_{\rho_{ij} \in [-1,1]} \left| C_{ij} - \int_{[0,1]^2} F_i^{-1}(u_i) F_j^{-1}(u_j) p_{\mathbf{u}}(u_i, u_j; \rho_{ij}) du_i du_j \right| \quad j > i. \quad (56)$$

Once all off-diagonal entries of  $\mathbf{R}$  are computed in this way, we can assemble the symmetric matrix

$$\mathbf{R} = \begin{bmatrix} 1 & \rho_{12} & \cdots & \rho_{1n} \\ \rho_{12} & 1 & \cdots & \rho_{2n} \\ \vdots & & \ddots & \vdots \\ \rho_{1n} & \rho_{2n} & \cdots & 1 \end{bmatrix}. \quad (57)$$

<sup>3</sup>Recall that

$$\frac{dG^{-1}(G(x))}{dx} = 0 \quad \Rightarrow \quad \frac{dG^{-1}(u)}{du} = \frac{1}{G'(G^{-1}(u))} = \frac{1}{p(G^{-1}(u))}. \quad (49)$$

This explains the term  $\mathbf{z}_{\mathbf{u}} \mathbf{I} \mathbf{z}_{\mathbf{u}}^T$  in (50).

<sup>4</sup>Recall that, by definition, the covariance of a Gaussian copula has ones along the diagonal (variances are one). This implies that the off-diagonal entries of  $\mathbf{R}$  coincide with the correlation coefficients  $\rho_{ij}$ , i.e.,

$$R_{ij} = \begin{bmatrix} 1 & \rho_{ij} \\ \rho_{ij} & 1 \end{bmatrix} \quad (55)$$

Of course  $\mathbf{R}$  may not be positive definite. The reason is that a greedy optimization procedure was used to compute each entry of  $\mathbf{R}$  independently. The closest positive definite matrix  $\mathbf{R}^+$  to  $\mathbf{R}$  in the Frobenius norm can be easily obtained by performing a spectral decomposition of  $\mathbf{R}$  and setting all negative eigenvalues to zero.

$$\mathbf{R} = \mathbf{V}\mathbf{\Lambda}\mathbf{V}^T \Rightarrow \mathbf{R}^+ = \mathbf{V}\mathbf{\Lambda}^+\mathbf{V}^T \quad \mathbf{\Lambda}^+ = \max\{\mathbf{\Lambda}, \mathbf{0}\}. \quad (58)$$

The transformation between correlated Gaussian copula variable  $\mathbf{u}$  (with correlation  $\mathbf{R}$ ) and the output vector  $\mathbf{g}$  with given marginal distributions  $p(g_j)$  and correlation  $\mathbf{C}$  is known as *Nataf transformation*.

## 6.2. Sampling from Gaussian copulas

The procedure to sample from a Gaussian copula is very simple:

1. We first sample realizations of a Gaussian vector with zero mean and unit variance, say  $\mathbf{h}^{(j)}$ .
2. Such sample vectors are then transformed to a vector with correlation  $\mathbf{R}$  (copula correlation) using the Cholesky factor<sup>5</sup> of  $\mathbf{R}$ . Call such samples  $\mathbf{s}^{(j)} = \mathbf{L}\mathbf{f}^{(j)}$  ( $\mathbf{L}$  is the lower-triangular Cholesky factor of  $\mathbf{R}$ ).
3. Each component of the rotated vectors is then mapped to a uniform distribution via the Gaussian probability mapping  $F_g$  (which is the same for all components), i.e.,  $\mathbf{u}^{(i)} = F_g(\mathbf{s}^{(j)})$ . The samples  $\mathbf{u}^{(j)}$  are samples of the Gaussian copula.
4. At this point we generate a sample of the random vector of interest as  $\mathbf{g}$  by using the marginal CDF mapping as

$$\mathbf{g}^{(i)} = \left[ F_1^{-1}\left(u_1^{(i)}\right), \dots, F_{N_y}^{-1}\left(u_{N_y}^{(i)}\right) \right]. \quad (60)$$

Here,  $F_i^{-1}$  is the inverse CDF of the random variable  $g_i$ , which we easily obtain from the PDF  $p(g_i)$  (see Eq. (32)).

## 7. Numerical results

In this section, we apply the uncertainty quantification methods developed in this paper to the *nonlinear* integro-differential operator

$$g(y) = \mathcal{N}(f) = \int_{-1}^1 (f(x)y + f(x)f'(x) \sin(\pi y^2) \cos(x)) dx. \quad (61)$$

To this end, we first approximate  $g(y) = \mathcal{N}(f(x))$  using a feed-forward neural network trained on a large dataset of input-output pairs  $\{f(x), g(y)\}$  via a standard discrete  $L_2$  performance metric. The input and output functions are discretized on a Gauss-Legendre-Lobatto grid [5] with  $N_x = N_y = 31$  points in  $[-1, 1]$ . This allows us to use high-order approximations of both the derivative and the integral appearing in (61). The ensemble of input functions is constructed by sampling the  $N_x$ -dimensional input vector  $\mathbf{f}$  representing  $f(x)$  from a probability distribution with Gaussian i.i.d. components. We also consider a separate neural

---

<sup>5</sup>The matrix  $\mathbf{R}$  is symmetric and positive definite. Hence it admits the Cholesky factorization  $\mathbf{R} = \mathbf{L}\mathbf{L}^T$  where  $\mathbf{L}$  is lower triangular with positive diagonal entries. If  $\mathbf{f}$  is a Gaussian vector with zero mean and unit covariance then  $\mathbf{s} = \mathbf{L}\mathbf{f}$  is a Gaussian vector with zero mean and covariance  $\mathbf{R}$ . In fact

$$\mathbb{E} \{ \mathbf{s}\mathbf{s}^T \} = \mathbf{L}\mathbb{E} \{ \mathbf{f}\mathbf{f}^T \} \mathbf{L}^T = \mathbf{L}\mathbf{L}^T = \mathbf{R}. \quad (59)$$

Nonlinear Operator				
Layers	Number of Samples	Batch Size	Epochs	Learning Rate
1 Layer	1 M	2000	1000	0.01
5 Layers	1 M	1000	300	0.01
20 Layers	1 M	2000	900	0.01

Linear Operator				
Layers	Number of Samples	Batch Size	Epochs	Learning Rate
1 Layer	1 M	1000	5000	0.001
5 Layers	1 M	1000	100	0.001
20 Layers	1 M	1000	200	0.001

Table 1: Number of layers, number of input-output samples, and optimization parameters used to train the feed-forward neural networks approximating the operators (61) and (62). The ADAM optimizer was used for training. The number of neurons is fixed at  $N = 64$  in each layer.

network approximating a simplified version of the previous operator, namely, a *linear* integro-differential operator

$$g(y) = \mathcal{L}f = \int_{-1}^1 (f(x)y + f'(x) \sin(\pi y^2) \cos(x)) dx. \quad (62)$$

In Table 1 we summarize the set of optimization parameters we used to train both neural networks via the ADAM optimizer.

### 7.1. Input functions perturbed by random noise

With a fully trained neural network available, we now consider an input vector of the form  $\mathbf{f} = \boldsymbol{\mu} + \mathbf{z}$ , where  $\boldsymbol{\mu}$  is *fixed* and  $\mathbf{z}$  is a random perturbation drawn from the uniform probability distribution defined in (5), with varying perturbation amplitudes  $\beta$ . In Figure 4, we plot the Lagrange polynomial interpolating the mean vector  $\boldsymbol{\mu}$ , along with several random realizations of  $f(x)$  i.e., Lagrange polynomials interpolating random input vectors of the form  $\boldsymbol{\mu} + \mathbf{z}$ , for different values of  $\beta$ .

### 7.2. PDF of the neural network output and its statistical moments

In this section, we study the accuracy of the linearized leaky ReLU approximation of the PDF and the statistical moments. To this end, we first generate 100,000 realizations of the random input functions  $f(x)$  shown in Figure 4 (i.e., 100,000 samples of the random vector  $\mathbf{f} = \boldsymbol{\mu} + \mathbf{z}$ ), and compute a Monte Carlo (MC) approximation of the statistical properties of the neural network output, for both nonlinear and linear operators in equations (62) and (61), respectively. In Figure 5 we plot one- and two-point joint PDFs of  $g_1, g_6, g_{11}, g_{16}, g_{21}$  (components of the output vector  $\mathbf{g}$ ) generated by the benchmark MC simulation. In Figures 6 and 7, we compare the Monte Carlo benchmark results with the approximate PDFs obtained from the linearized leaky ReLU approximation, i.e., Eq. (32), in the case of the nonlinear operator. For noise amplitudes  $\beta \geq 1$ , we observe a slight discrepancy between MC and the analytical PDFs. Specifically, the distributions begin to deviate from a fully symmetric bell-shaped form and exhibit heavier tails in some regions, although in other regions the close agreement observed in the linear case still holds. These results are independent of the number of layers considered in the feed-forward neural network as demonstrated in Figure 8.

Despite these slight deviations, the statistical moments of the output obtained from the linearized leaky ReLU approximation – namely, the mean (37), variance (41), and covariance (42) – remain highly accurate, exhibiting strong agreement with the corresponding moments computed with MC (see Table 2).

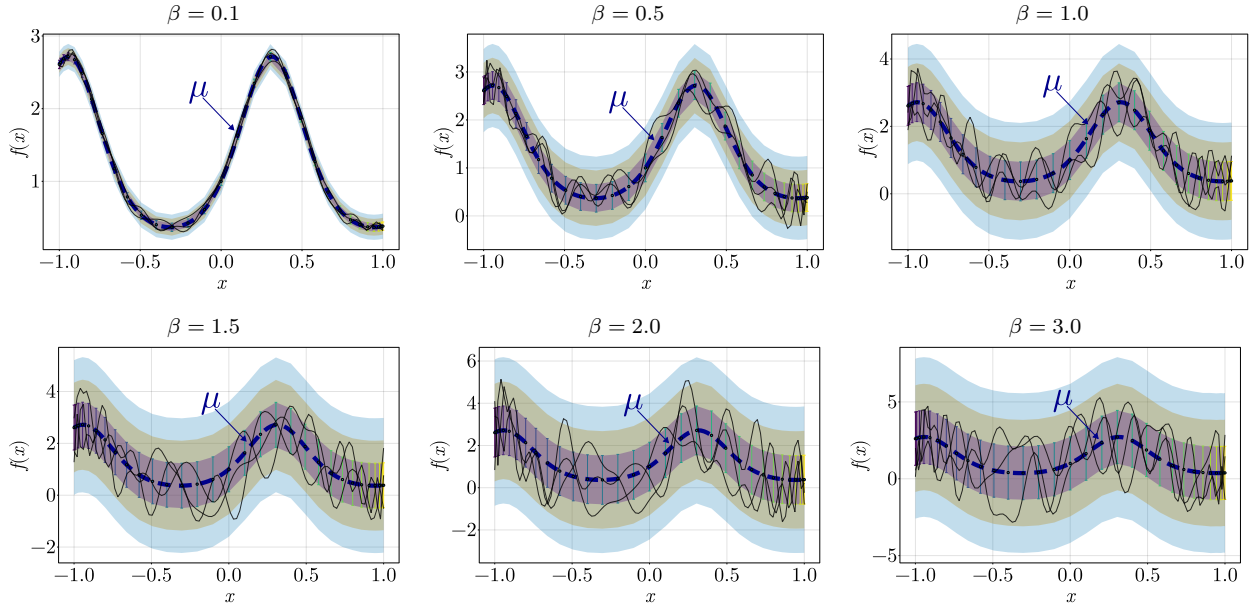


Figure 4: Samples of the random input function  $f(x)$  for fixed mean and different perturbation amplitudes  $\beta$ . Shown are the Lagrange polynomial interpolating the mean vector  $\mu$ , along with several random realizations of  $f(x)$ , i.e., Lagrange polynomials interpolating input vectors of the form  $\mu + \mathbf{z}$ , where  $\mathbf{z}$  is a random vector with i.i.d. uniform components in  $[-\beta, \beta]$  (see Eq. (5)).

$\beta = 1.5$	$g_6$	$g_{11}$	$g_{16}$	$g_{21}$
$g_1$	0.32(0.32)	0.21(0.21)	0.17(0.15)	-0.19(-0.19)
$g_6$		0.99(0.99)	-0.77(-0.73)	0.87(0.87)
$g_{11}$			-0.82(-0.77)	0.92(0.92)
$g_{16}$				-0.89(-0.84)

Table 2: Nonlinear operator (61). Correlation coefficients computed from analytical expression of moments derived from the linearized leaky ReLU approximation method compared to those numerically found from MC simulations (in parentheses). See Figure 5 for a plot of two-point PDFs of  $g_i$  and  $g_j$ .

On the other hand, in Figure 9 we observe excellent good agreement between the PDFs computed numerically and those obtained from the analytical approximation in the case of the linear operator, regardless of the number of layers used in training the neural network, and for significantly large perturbation amplitude.

The reason behind the surprisingly accurate PDFs and statistical moments obtained from the linearized leaky ReLU network approximation lies in the manner in which the approximation error propagates through the layers of the network (see Appendix B). In Figure 10, we plot the PDF of the error defined in (B.10), obtained via Monte Carlo sampling. As expected, the numerical results show that the error is proportional to the perturbation amplitude in the input vector. Furthermore, the error seems to decrease with the number of neural network layers  $L$ . This suggests that linearized leaky ReLU approximations of MLP networks are most effective for deep networks.

### 7.3. Gaussian copula PDF surrogates

In this section we study the accuracy of Gaussian copulas to approximate the *full* joint PDF  $p(\mathbf{g})$  of the neural network output. As discussed in section 6, a Gaussian copula can be constructed using the marginal PDFs  $p(g_j)$  and the correlation function  $\mathbb{E}\{g_i g_j\}$ . These quantities can accurately approximated by the analytical expressions in (32) and (40). In Figure 11, we show that the entries of the correlation matrix  $\mathbb{E}\{g_i g_j\}$  obtained by the MC benchmark and the Gaussian copula for the nonlinear operator are

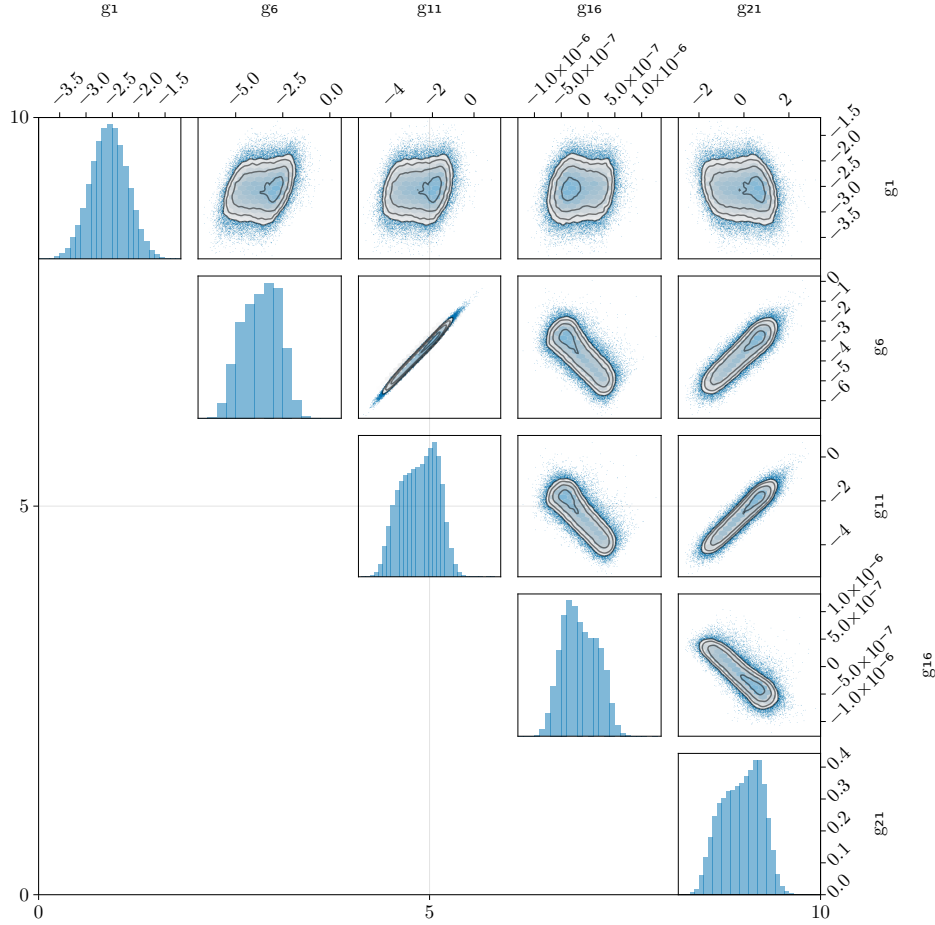


Figure 5: Nonlinear operator (61). Corner plot of the one- and two-point PDFs of  $g_1, g_6, g_{11}, g_{16}, g_{21}$  generated by MC simulation.

nealy identical, suggesting proper training of the copula. In Figures 12 and 13, we compare various two-point PDFs of the neural network output obtained from the Monte Carlo benchmark and the Gaussian copula approximation, for the linear and nonlinear operators, respectively. It is seen that such PDFs are in excellent agreement.

## 8. Summary

We presented new methods for uncertainty propagation in feed-forward neural network architectures with leaky ReLU activation functions, subject to random perturbations in the input vectors. In particular, we derived computable approximate analytical expressions for the probability density function (PDF) of the neural network output and its statistical moments. To obtain these expressions, we introduced a suitable linearization of the leaky ReLU activation functions, which renders the formulas for both the PDF and the moments analytically tractable. We applied these formulas to feed-forward neural networks trained to approximate linear and nonlinear integro-differential operators, and found that the resulting statistical predictions (PDFs and statistical moments) remain remarkably accurate even for large perturbation amplitudes in the input vectors. The accuracy of the PDFs and statistical moments obtained from the linearized leaky ReLU network approximation can be attributed to the way the approximation error propagates through the

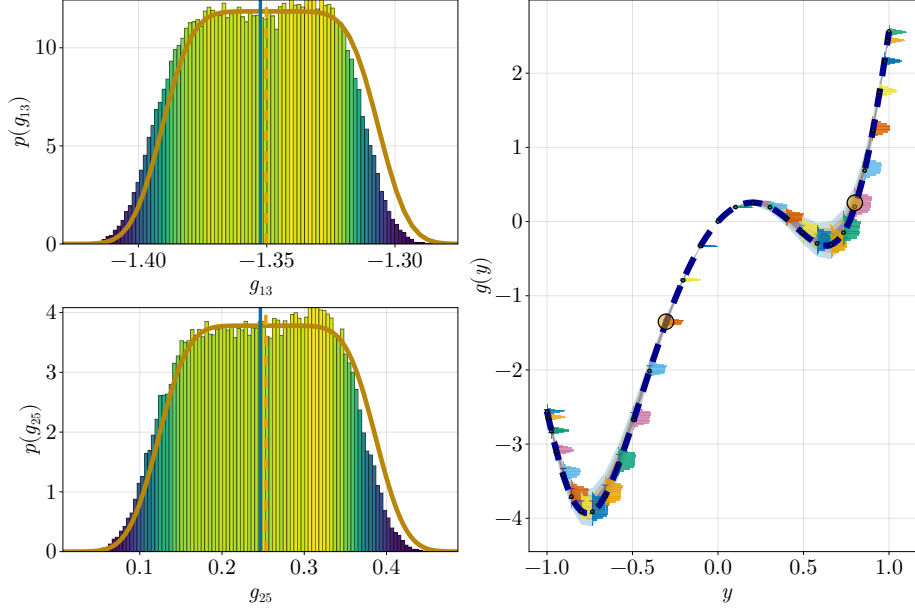


Figure 6: Nonlinear operator (61). Comparison between the PDFs of  $g_{13}$  and  $g_{25}$  as predicted by (32) (yellow curve – linearized leaky ReLU approximation) and the Monte Carlo benchmark. The perturbation amplitude in the input function here is set to  $\beta = 0.1$  (see Figure 4). We also plot the confidence intervals  $\pm\kappa\sigma$  ( $\kappa = 1, 2, 3$ ) representing the variability of the output  $g(y)$  relative to the mapped mean input function.

network layers (see (Appendix B)). Specifically, we found that the error is proportional to the perturbation amplitude in the input vector and tends to decrease with the number of network layers  $L$ , suggesting that linearized leaky ReLU approximations are particularly effective for deep networks. We also investigated the accuracy of Gaussian copula models for approximating the *full* joint PDF  $p(\mathbf{g})$  of the neural network output. As discussed in Section 6, a Gaussian copula can be constructed using the marginal PDFs  $p(g_j)$  and the correlation function  $\mathbb{E}\{g_i g_j\}$ , both of which are accurately approximated by the analytical expressions derived in (32) and (40). This enables a fully analytical construction of the Gaussian copula surrogate model for the PDF of the neural network output. Our results show that this model yields highly accurate approximations of two-point and three-point PDFs, indicating that the Gaussian copula serves as an excellent surrogate for the joint distribution of the neural network output. The methods we proposed in this work can be extended to neural operator architectures, such as Fourier Neural Operators (FNOs) [10] or DeepONets [19, 6]. These architectures which can be viewed as generalizations of the multilayer perceptron (MLP) networks considered in this study [2, 7].

## Acknowledgements

This work was supported by the U.S. Department of Energy (DOE) under grant “Resolution-invariant deep learning for accelerated propagation of epistemic and aleatory uncertainty in multi-scale energy storage systems, and beyond,” contract number DE-SC0024563.

## Appendix A. Derivation of the PDF of the neural network output

In this appendix, we derive an analytical expression for the probability density function (PDF) of each component of the neural network output, under the assumption that the random input vector is uniformly distributed (see (5)). To simplify the calculation, we linearize the leaky ReLU activation functions around

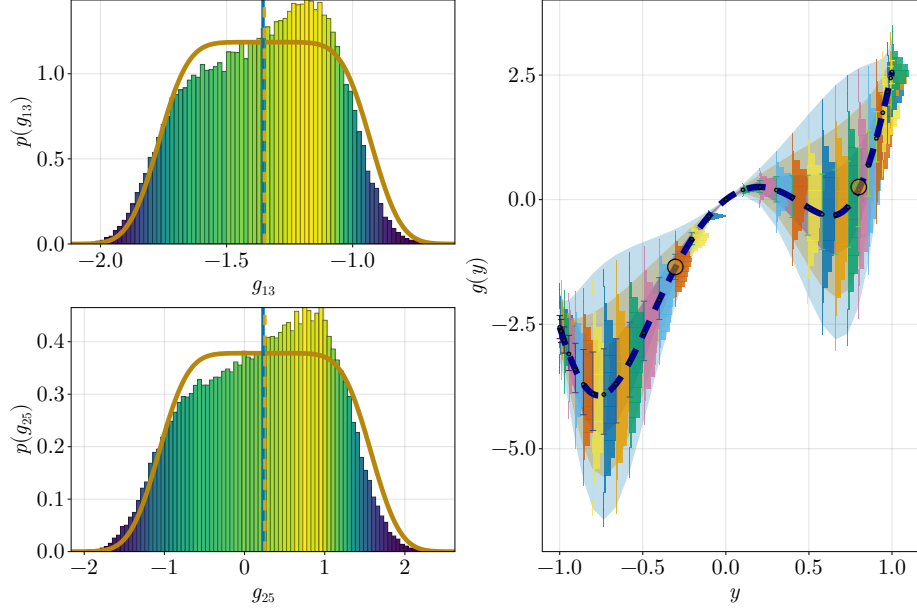


Figure 7: Nonlinear operator (61). Comparison between the PDFs of  $g_{13}$  and  $g_{25}$  as predicted by (32) (yellow curve – linearized leaky ReLU approximation) and the Monte Carlo benchmark. The perturbation amplitude in the input function here is set to  $\beta = 1$  (see Figure 4). We also plot the confidence intervals  $\pm\kappa\sigma$  ( $\kappa = 1, 2, 3$ ) representing the variability of the output  $g(y)$  relative to the mapped mean input function.

the mean of the input vector  $\mu$  (see (27) and (29)). Let us first consider the case of a neural network with a single layer. Substituting equations (5) and (27) into (20), we obtain the following expression for the PDF of  $g_j$

$$\begin{aligned}
 p(g_j) &= \frac{1}{2\pi} \frac{1}{(2\beta)^{N_x}} \int_{-\infty}^{\infty} \int_{[-\beta, \beta]^{N_x}} e^{ia_j(g_j - \mathbf{A}_j \cdot [\phi(\mathbf{W}_1 \mu + \mathbf{b}_1) + \mathbf{J}_1 \mathbf{z}])} d\mathbf{z} da_j, \\
 &= \frac{1}{2\pi} \frac{1}{(2\beta)^{N_x}} \int_{-\infty}^{\infty} e^{ia_j[g_j - \mathbf{A}_j \cdot \phi(\mathbf{W}_1 \mu + \mathbf{b}_1)]} \left[ \int_{[-\beta, \beta]^{N_x}} e^{ia_j \mathbf{A}_j \mathbf{J}_1 \mathbf{z}} d\mathbf{z} \right] da_j. \tag{A.1}
 \end{aligned}$$

where  $\mathbf{A}_j$  is the  $j$ -th row of the matrix  $\mathbf{A}$  (output weights), and  $\mathbf{J}_1$  is the matrix defined in (28). Upon definition of the  $N_x$ -dimensional row vector

$$\mathbf{q}_j = \mathbf{A}_j \mathbf{J}_1, \tag{A.2}$$

we have

$$\begin{aligned}
 \int_{[-\beta, \beta]^{N_x}} e^{ia_j \mathbf{q}_j \cdot \mathbf{z}} d\mathbf{z} &= \prod_{n=1}^{N_x} \int_{-\beta}^{\beta} e^{-ia_j q_{jn} z_n} dz_n \\
 &= \prod_{n=1}^{N_x} \frac{e^{ia_j \beta q_{jn}} - e^{-ia_j \beta q_{jn}}}{ia_j q_{jn}} \\
 &= \prod_{n=1}^{N_x} \frac{2\beta \sin(a_j \beta q_{jn})}{a_j q_{jn}} \\
 &= \prod_{n=1}^{N_x} 2\beta \text{sinc}(a_j \beta q_{jn}), \tag{A.3}
 \end{aligned}$$

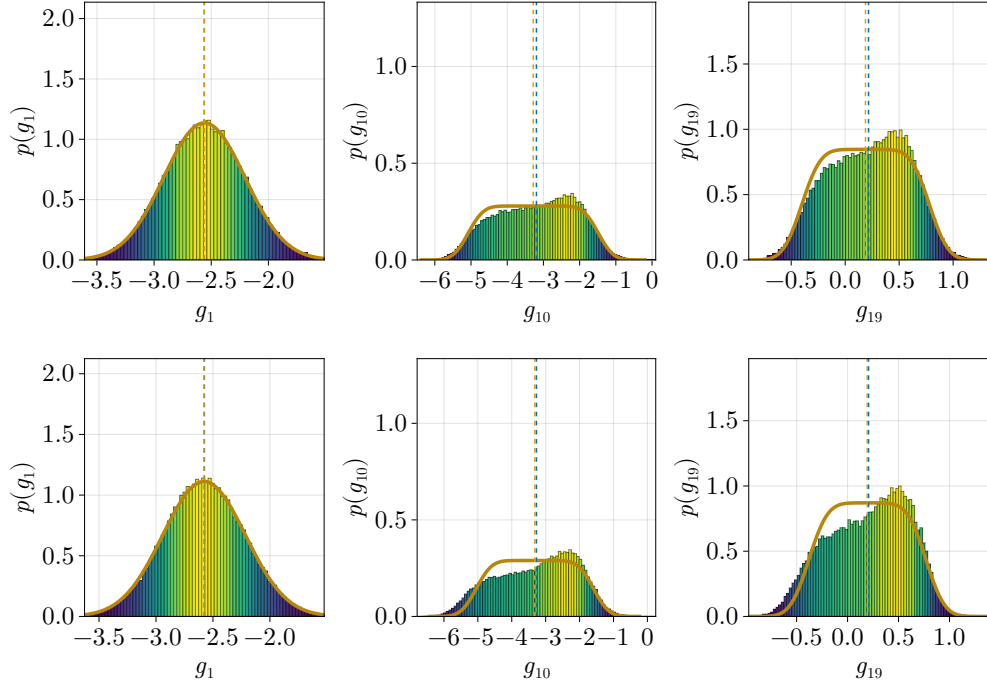


Figure 8: Nonlinear operator (61). Marginal PDFs of the output function as a function of the number of layers. Shown are results for 1 layer (first row) and 20 layers (last row). The noise amplitude here is set to  $\beta = 1.5$ .

where  $\text{sinc}(\cdot)$  is the sinc function. Substituting (A.3) into (A.1) yields

$$p(g_j) = \frac{1}{2\pi} \frac{1}{(2\beta)^{N_x}} \int_{-\infty}^{\infty} e^{ia_j[g_j - \mathbf{A}_j \cdot \phi(\mathbf{W}_1 \boldsymbol{\mu} + \mathbf{b}_1)]} \prod_{n=1}^{N_x} 2\beta \text{sinc}(a_j \beta q_{jn}) da_j. \quad (\text{A.4})$$

Finally, by using the Fourier convolution theorem we obtain

$$p(g_j) = \frac{1}{2\pi} \left( \prod_{n=1}^{N_x} \frac{2\pi}{q_{jn}} \right) \Pi_{\beta q_{j1}}[\eta(g_j)] * \dots * \Pi_{\beta q_{jN_x}}(\eta(g_j)) \quad (\text{A.5})$$

where

$$\eta(g_j) = g_j - \mathbf{A}_j \cdot \phi(\mathbf{W}_1 \boldsymbol{\mu} + \mathbf{b}_1), \quad (\text{A.6})$$

\* denotes a standard convolution operation, and  $\Pi_{\beta q_{j1}}(\cdot)$  is the rectangular function<sup>6</sup>

$$\Pi_{\beta q_{j1}}(x) = H(x + \beta q_{j1}) - H(x - \beta q_{j1}). \quad (\text{A.7})$$

In practice, one may compute  $p(g_j)$  using its inverse Fourier transform representation, which involves the product of  $\text{sinc}(\cdot)$  functions in (A.4), rather than through the iterated convolution of rectangular functions, which can be more computationally expensive.

## Appendix B. Error analysis for neural networks with linearized leaky ReLU activation functions

In this appendix, we develop a thorough error analysis to quantify the effects of linearizing leaky ReLU activation functions on the neural network output. This analysis provides insight into why the approximate

<sup>6</sup>In equation (A.7),  $H(x)$  denotes the Heaviside step function.

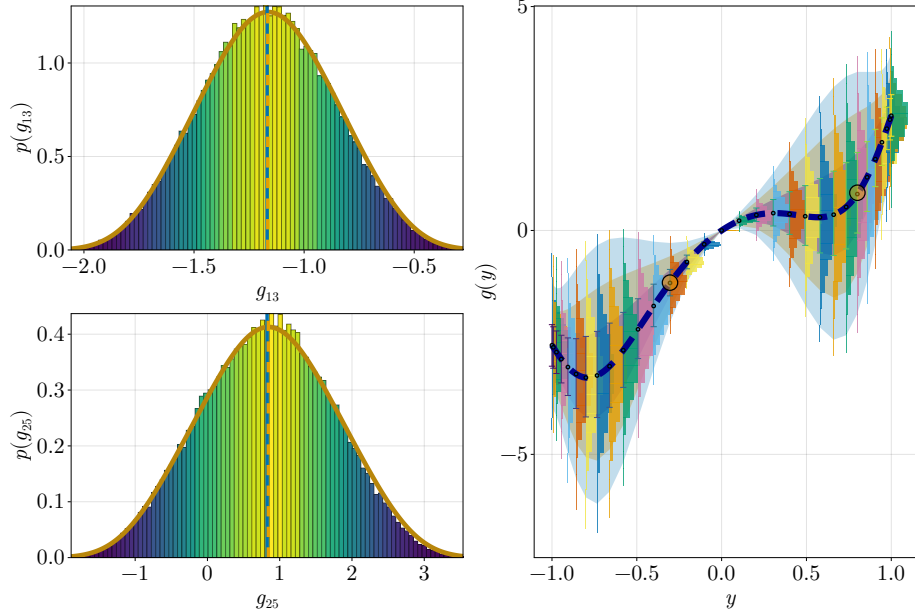


Figure 9: Linear operator (62). Comparison between the PDFs of  $g_{13}$  and  $g_{25}$  as predicted by (32) (yellow curve – linearized leaky ReLU approximation) and the Monte Carlo benchmark. The perturbation amplitude in the input function here is set to  $\beta = 2$  (see Figure 4). We also plot the confidence intervals  $\pm \kappa \sigma$  ( $\kappa = 1, 2, 3$ ) representing the variability of the output  $g(y)$  relative to the mapped mean input function.

analytical formulas for the marginal probability density function (PDF) we obtained in Section 4.2, and the formulas for the statistical moments in Section 5, remain accurate even in the presence of large perturbation amplitudes in the input vectors  $\mathbf{f} = \boldsymbol{\mu} + \mathbf{z}$ , i.e., large perturbation amplitudes in  $\mathbf{z}$ .

Hereafter, we are going to *analyze* the error behavior as it is pushed-forward into the neural net. To this end, let us first recall the linear approximation of first neural network layer, as discussed in section 4.2

$$\phi(\mathbf{W}_1(\boldsymbol{\mu} + \mathbf{z}) + \mathbf{b}_1) \simeq \phi(\mathbf{h}_1) + \mathbf{J}_1(\mathbf{h}_1)\mathbf{z}, \quad (\text{B.1})$$

where

$$\mathbf{h}_1 = \mathbf{W}_1\boldsymbol{\mu} + \mathbf{b}_1, \quad \text{and} \quad \mathbf{J}_1(\mathbf{h}_1) = \phi'(\mathbf{h}_1) \square \mathbf{W}_1. \quad (\text{B.2})$$

Equation (B.1) can be equivalently written as<sup>7</sup>

$$\phi(\mathbf{h}_1 + \mathbf{W}_1\mathbf{z}) \simeq \phi'(\mathbf{h}_1) \circ [\mathbf{h}_1 + \mathbf{W}_1\mathbf{z}]. \quad (\text{B.3})$$

This expression is exact if the sign of  $\mathbf{h}_1$  matches the sign of  $\mathbf{h}_1 + \mathbf{W}_1\mathbf{z}$  component-wise. In this case, the perturbation  $\mathbf{z}$  is not large enough to push  $\mathbf{h}_1 + \mathbf{W}_1\mathbf{z}$  to the other side of the leaky ReLU activation function, thereby rendering the linear expansion (B.3) exact. Given the "half" linearity of the leaky ReLU activation function, it is straightforward to compute the exact residual in (B.3), i.e., the *exact error* incurred by replacing  $\phi(\mathbf{W}_1(\boldsymbol{\mu} + \mathbf{z}) + \mathbf{b}_1)$  with the linear approximation  $\phi(\mathbf{h}_1) \circ [\mathbf{h}_1 + \mathbf{W}_1\mathbf{z}]$ . We have

$$\phi(\mathbf{h}_1 + \mathbf{W}_1\mathbf{z}) = \phi'(\mathbf{h}_1) \circ [\mathbf{h}_1 + \mathbf{W}_1\mathbf{z}] + \underbrace{(\phi'(\mathbf{h}_1 + \mathbf{W}_1\mathbf{z}) - \phi'(\mathbf{h}_1)) \circ [\mathbf{h}_1 + \mathbf{W}_1\mathbf{z}]}_{\Delta\phi_1(\mathbf{h}_1)}. \quad (\text{B.4})$$

<sup>7</sup>In equation (B.3)  $\circ$  denotes the Hadamard matrix product.

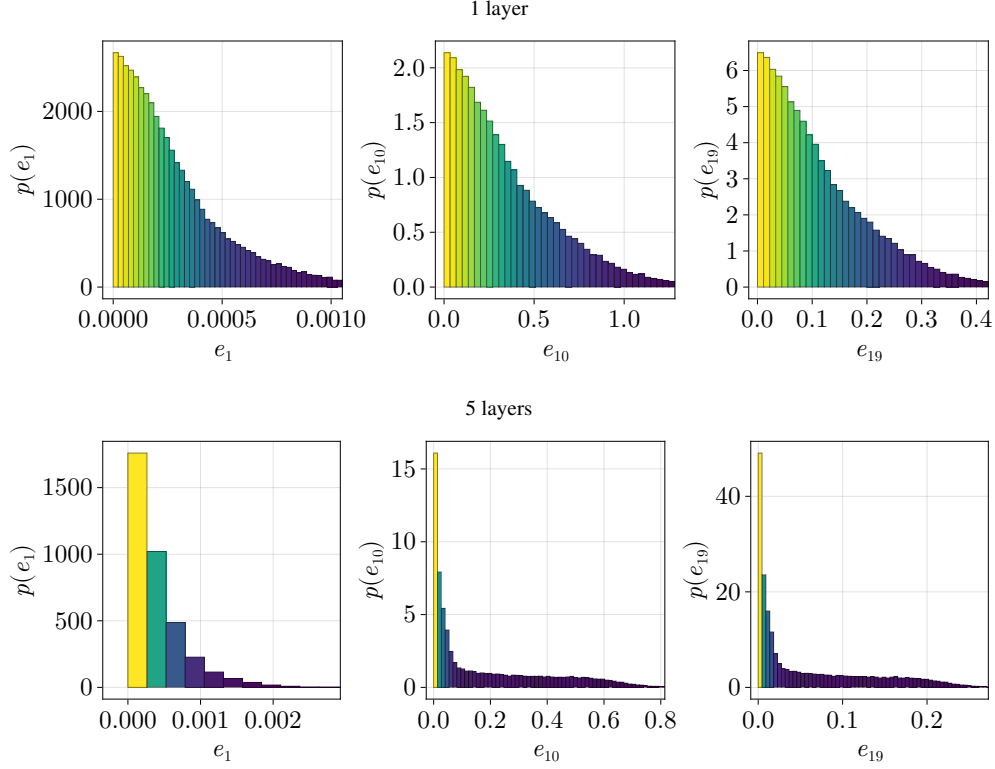


Figure 10: Nonlinear operator (61). PDFs of the error (B.10) for noise amplitude  $\beta = 1.5$  and different number of layers. It is seen that as the number of layer increases the PDF of the error tends to concentrate around zero. This suggests that that linearized leaky ReLU approximations of MLP networks are most effective for deep networks.

We can now proceed recursively across the neural network and quantify the error in the output of subsequent layers, which has two components: i) the error in the output of the previous layer passed through as input to the current layer, and error in the current layer output due to leaky ReLU linearization approximation. To quantify these errors we define recursively for  $n = 2, \dots, L$  and  $\mathbf{z}_1 = \mathbf{z}$

$$\mathbf{h}_n = \mathbf{W}_n \phi'(\mathbf{h}_{n-1}) \circ \mathbf{h}_{n-1} + \mathbf{b}_n, \quad (\text{B.5})$$

$$\mathbf{z}_n = \phi'(\mathbf{h}_{n-1}) \circ \mathbf{W}_{n-1} \mathbf{z}_{n-1} + \Delta \phi_{n-1}(\mathbf{h}_{n-1}), \quad (\text{B.6})$$

where

$$\Delta \phi_{n-1}(\mathbf{h}_{n-1}) = [\phi'(\mathbf{h}_{n-1} + \mathbf{W}_{n-1} \mathbf{z}_{n-1}) - \phi'(\mathbf{h}_{n-1})] \circ (\mathbf{h}_{n-1} + \mathbf{W}_{n-1} \mathbf{z}_{n-1}). \quad (\text{B.7})$$

This allows us to write the exact output of the  $L$ -th layer as

$$\phi(\mathbf{h}_L + \mathbf{W}_L \mathbf{z}_L) = \phi'(\mathbf{h}_L) \circ [\mathbf{h}_L + \mathbf{W}_L \mathbf{z}_L] + \Delta \phi_L(\mathbf{h}_L), \quad (\text{B.8})$$

where

$$\Delta \phi_L(\mathbf{h}_L) = [\phi'(\mathbf{h}_L + \mathbf{W}_L \mathbf{z}_L) - \phi'(\mathbf{h}_L)] \circ (\mathbf{h}_L + \mathbf{W}_L \mathbf{z}_L). \quad (\text{B.9})$$

Correspondingly, the error in the neural network output layer due to the linearized leaky ReLU approximation throughout the network is

$$\mathbf{e}(\mathbf{g}) = |\mathbf{A} \Delta \phi_L(\mathbf{h}_L)|, \quad (\text{B.10})$$

where  $\mathbf{A}$  are the output matrix.

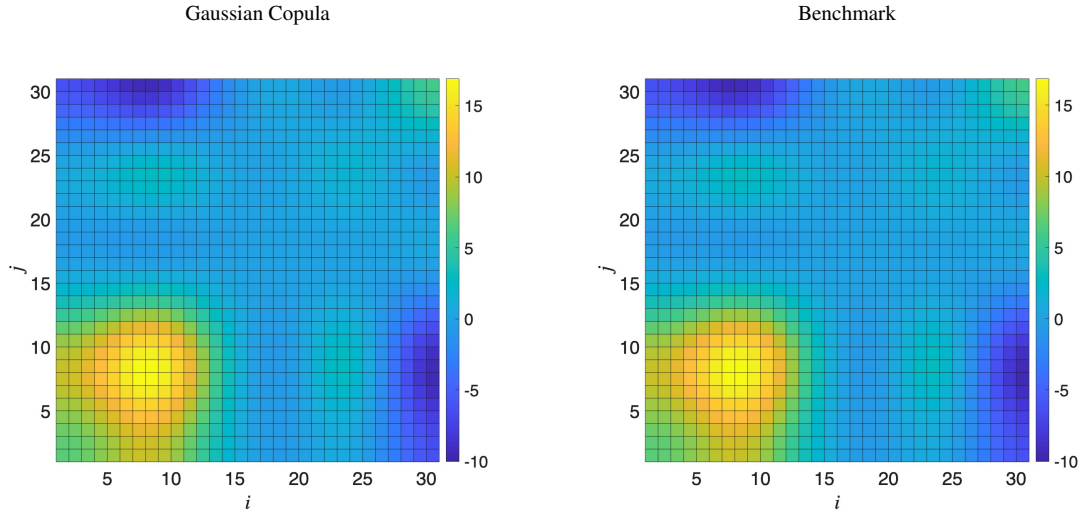


Figure 11: Nonlinear Operator (61). Comparison between the correlation matrix  $\mathbb{E}\{g_i g_j\}$  obtained from the Gaussian copula vs. the benchmark correlation obtained from MC.

## References

- [1] M. Abdar, F. Pourpanah, S. Hussain, D. Rezazadegan, L. Liu, M. Ghavamzadeh, P. Fieguth, X. Cao, A. Khosravi, U. R. Acharya, V. Makarenkov, and S. Nahavandi. A review of uncertainty quantification in deep learning: Techniques, applications and challenges. *Information Fusion*, 76:243–297.
- [2] N Boullé and A. Townsend. A mathematical guide to operator learning. In S. Mishra and A. Townsend, editors, *Handbook of Numerical Analysis, Vol 25*, pages 83–125. North-Holland, 2024.
- [3] C. Czado. *Analyzing dependent data with vine copulas*. Springer, 2019.
- [4] J. Gawlikowski, C. R. N. Tassi, M. Ali, J. Lee, M. Humt, J. Feng, A. Kruspe, R. Triebel, P. Jung, R. Roscher, M. Shahzad, W. Yang, R. Bamler, and X. X. Zhu. A survey of uncertainty in deep neural networks. *Artificial Intelligence Review*, 56(1), 2023.
- [5] J. S. Hesthaven, S. Gottlieb, and D. Gottlieb. *Spectral methods for time-dependent problems*, volume 21 of *Cambridge Monographs on Applied and Computational Mathematics*. Cambridge University Press, Cambridge, 2007.
- [6] G. E. Karniadakis, I. G. Kevrekidis, L. Lu, P. Perdikaris, S. Wang, and L. Yang. Physics-informed machine learning. *Nature Reviews Physics*, 3:422–440, 2021.
- [7] N. Kovachki, Z. Li, B. Liu, K. Azizzadenesheli, K. Bhattacharya, A. Stuart, and A. Anandkumar. Neural operator: Learning maps between function spaces. *The Journal of Machine Learning Research*, 24(1):4061–4157.
- [8] P. Lambrianides, Q. Gong, and D. Venturi. A new scalable algorithm for computational optimal control under uncertainty. *J. Comput. Phys.*, 420:109710, 2020.
- [9] Q. Li, T. Lin, and Z. Shen. Deep learning via dynamical systems: An approximation perspective. *J. Eur. Math. Soc.*, (published online first), 2022.

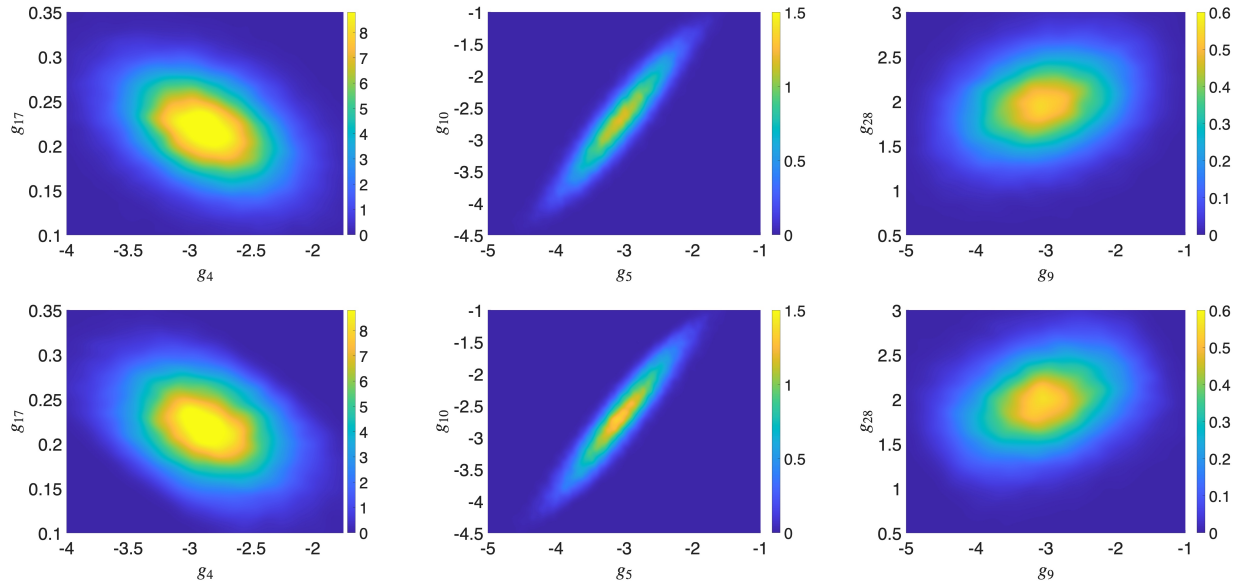


Figure 12: Linear Operator (62). Comparison of the 2-point PDFs generated by Gaussian copula (top) vs. the benchmark 2-point PDFs obtained from MC.

- [10] Z. Li, N. Kovachki, K. Azizzadenesheli, B. Liu, K. Bhattacharya, A. Stuart, and A. Anandkumar. Fourier neural operator for parametric partial differential equations. In *ICLR*, pages 1–16, 2021.
- [11] X. Meng, Z. Zhen, D. Zhang, and G. Karniadakis. Ppinn: Parareal physics-informed neural network for time-dependent pdes. *Comput. Methods in Appl. Mech. Eng.*, 370:113250, 2020.
- [12] T. Miyagawa and T. Yokota. Physics-informed neural networks for functional differential equations: Cylindrical approximation and its convergence guarantees. *arXiv:2410.18153*, pages 1–75, 2024.
- [13] A. F. Psaros, X. Meng, Z. Zou, L. Guo, and G. E. Karniadakis. Uncertainty quantification in scientific machine learning: Methods, metrics, and comparisons. *Journal of Computational Physics*, 477:111902, 2023.
- [14] M. Raissi and G. E. Karniadakis. Hidden physics models: Machine learning of nonlinear partial differential equations. *J. Comput. Phys.*, 357:125–141, 2018.
- [15] D. Venturi. The numerical approximation of nonlinear functionals and functional differential equations. *Physics Reports*, 732:1–102, 2018.
- [16] D. Venturi, H. Cho, and G. E. Karniadakis. The Mori-Zwanzig approach to uncertainty quantification. In R. Ghanem, D. Higdon, and H. Owhadi, editors, *Handbook of uncertainty quantification*. Springer, 2016.
- [17] D. Venturi and A. Dektor. Spectral methods for nonlinear functionals and functional differential equations. *Res. Math. Sci.*, 8(27):1–39, 2021.
- [18] D. Venturi and X. Li. The Mori-Zwanzig formulation of deep learning. *Research in the Mathematical Sciences*, 10:1–47, 2023.
- [19] S. Wang, H. Wang, and P. Perdikaris. Learning the solution operator of parametric partial differential equations with physics-informed DeepONets. *Science Advances*, 7(40):1–27, 2021.

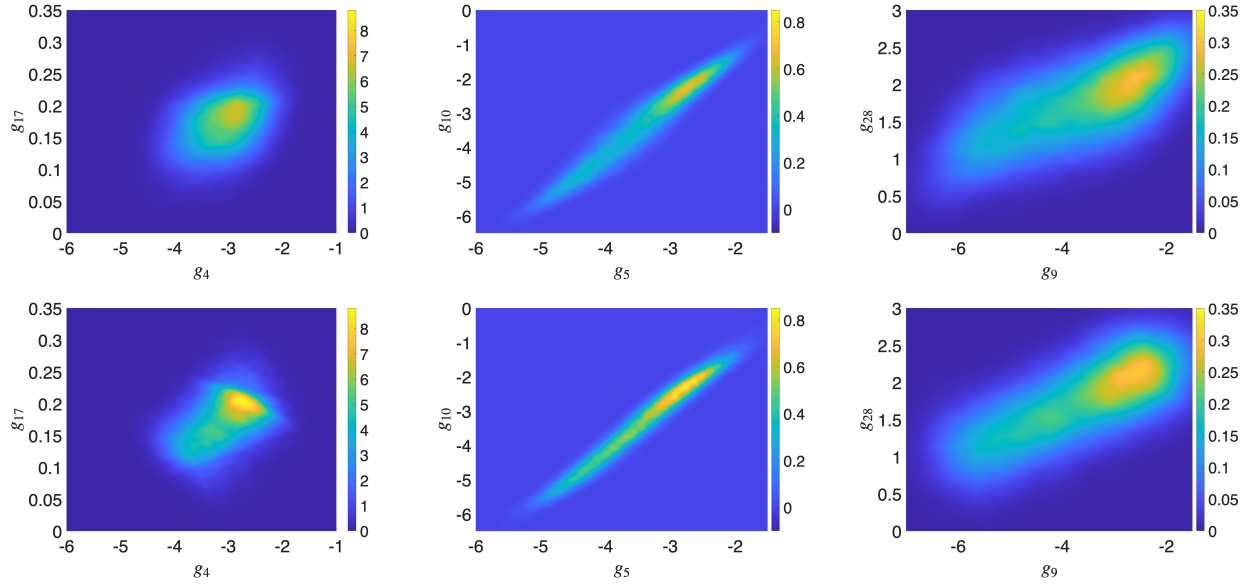


Figure 13: Nonlinear operator (61). Comparison of the 2-point PDFs generated by Gaussian copula (first row) vs. the benchmark 2-point PDFs obtained from MC (second row).

- [20] Z. Zou, X. Meng, and G. E. Karniadakis. Uncertainty quantification for noisy inputs–outputs in physics-informed neural networks and neural operators. *Computer Methods in Applied Mechanics and Engineering*, 433:117479, 2025.